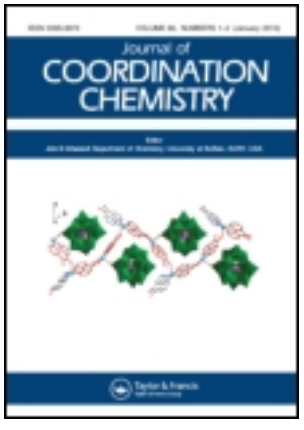

Journal of Coordination Chemistry
Publication details, including instructions for authors and subscription information:
http://www.tandfonline.com/loi/gcoo20

Synthesis, crystal structure, Hirshfeld surfaces, and spectral properties of Cu(II) and Co(II) complexes with 3-phenoxymethyl-4-phenyl-5-(2-pyridyl)-1,2,4-triazole

Yuan Li [a], Chen-Guang Zhang [a], Liang-Ying Cai [a] & Zuo-Xiang Wang [a]

[a] College of Chemistry and Chemical Engineering, Southeast University, Nanjing, P.R. China

Accepted author version posted online: 18 Jul 2013.Published online: 14 Aug 2013.

To cite this article: Yuan Li, Chen-Guang Zhang, Liang-Ying Cai & Zuo-Xiang Wang (2013) Synthesis, crystal structure, Hirshfeld surfaces, and spectral properties of Cu(II) and Co(II) complexes with 3-phenoxymethyl-4-phenyl-5-(2-pyridyl)-1,2,4-triazole, Journal of Coordination Chemistry, 66:17, 3100-3112, DOI: 10.1080/00958972.2013.826350

To link to this article: http://dx.doi.org/10.1080/00958972.2013.826350

Journal of Coordination Chemistry, 2013
Vol. 66, No. 17, 3100–3112, http://dx.doi.org/10.1080/00958972.2013.826350

Synthesis, crystal structure, Hirshfeld surfaces, and spectral properties of Cu(II) and Co(II) complexes with 3-phenoxymethyl-4-phenyl-5-(2-pyridyl)-1,2,4-triazole

YUAN LI, CHEN-GUANG ZHANG, LIANG-YING CAI and ZUO-XIANG WANG*

College of Chemistry and Chemical Engineering, Southeast University, Nanjing, P.R. China

(*final version received 19 June 2013; in final form 2 July 2013*)

A new asymmetrical substituted triazole, 3-phenoxymethyl-4-phenyl-5-(2-pyridyl)-1,2,4-triazole (**L**) and its complexes, *cis*-$[Cu_2\mathbf{L}_2Cl_4]\cdot 2CH_3CN$ (**1**) and *trans*-$[Co\mathbf{L}_2Cl_2]\cdot 2H_2O\cdot 2CH_3CN$ (**2**), have been synthesized and characterized by IR, single-crystal X-ray diffraction, thermogravimetric analyses and Hirshfeld surfaces. In the structure, two **L** are mainly stabilized by an intermolecular C–H···N hydrogen bond. In **1** (or **2**), each **L** involves a doubly-bidentate (or chelating bidentate) coordination mode through one pyridine and two nitrogens (or one) of triazole, respectively. Complex **1** has a distorted trigonal bipyramidal $[CuN_3Cl_2]$ core with two *cis* Cl^- while **2** shows a distorted octahedron $[CoN_4Cl_2]$ with two *trans* Cl^-. We also prepared molecular Hirshfeld surface and fingerprint plot for **L**, **1** and **2**, which revealed the influence of different metals on coordinate of **L**.

Keywords: Syntheses; Triazole; Crystal structures; Copper(II) complex; Cobalt(II) complex

1. Introduction

Attention has been paid to the synthesis of 1,2,4-triazoles and their derivatives due to important pharmacological activities, specific magnetic properties [1, 2] and a broad range of applications such as antitumor (aq), fungicide, weedicide, etc. [3]. Substituted 1,2,4-triazoles also have attracted widespread attention in coordination chemistry because of their rich and versatile coordination modes [4–6]. Some iron(II) complexes with substituted 1,2,4-triazoles show fascinating spin-crossover properties and can be used in molecular electronics such as information storage and switching materials [7–9].

Crystal design and crystal engineering, prediction and computation of molecular crystal structures through intermolecular interactions also have aroused attention [10–12]. The main approach is through Hirshfeld surfaces, a powerful tool for elucidating molecular crystal structures [13]. Hirshfeld surfaces is a space partitioning construct that summarizes the crystal packing into a single 3-D surface, and the surface can be reduced to a 2-D fingerprint plot, which summarizes the complex information on intermolecular interactions

*Corresponding author. Email: 101010062@seu.edu.cn

present in molecular crystals [12]. The principles of Hirshfeld surfaces and fingerprint plots are reported [11].

Although some 4-substituted 3,5-di(2-pyridyl)-1,2,4-triazoles and their metal complexes have been synthesized [5, 9, 14, 15], complexes with asymmetrically 3,4,5-triaryl-substituted 1,2,4-triazoles have been less studied [16]. In continuation of our investigation of asymmetrically substituted 1,2,4-triazoles [17, 18], we present here the syntheses of a new triazole ligand, 3-phenoxymethyl-4-phenyl-5-(2-pyridyl)-1,2,4-triazole (**L**), and its complexes, *cis*-$[Cu_2\mathbf{L}_2Cl_4]\cdot 2CH_3CN$ (**1**) and *trans*-$[Co\mathbf{L}_2Cl_2]\cdot 2H_2O\cdot 2CH_3CN$ (**2**). In this work, we compared crystal structures, spectroscopic properties, and also investigated the influence of different metals on the ligand in terms of intermolecular interactions by using Hirshfeld surfaces and fingerprint plots.

2. Experimental

2.1. *Materials and measurements*

All chemicals were of analytical grade and solvents were purified by conventional methods. **L** was synthesized according to our earlier reported method [17]. Melting points were determined using an X4 digital microscope melting point apparatus and were uncorrected. C, H and N analyses were performed on a Perkin–Elmer 240 analyzer. IR spectra were recorded from 4000 to 400 cm^{-1} using KBr pellets on a Vector22 Bruker spectrophotometer. ^1H NMR spectra were measured with a Bruker Avance 300 spectrometer at ambient temperature in $CDCl_3$ using TMS as the internal reference. Thermogravimetric analyses (TGA) were performed on a NETZSCH STA 449F3 thermal analyzer under nitrogen at 10 °C min^{-1}.

2.3. *Preparation of L*

3-phenoxymethyl-4-phenyl-5-(2-pyridyl)-1,2,4-triazole (**L**) was synthesized by the reaction of di(p-methylphenyl)phosphazoanilide (3.6 g, 16.5 mM) and *N*-phenoxyacetyl-*N*′-(2-pyridoyl)hydrazine (4.1 g, 15.0 mM) in *N*,*N*′-dimethylaniline (30 mL) at 190–200 °C for 3 h [19], yield 2.2 g (44.3%), m.p. 144–145 °C. White single crystals suitable for X-ray analysis were obtained from an ethyl acetate solution. Anal. Calcd for $C_{20}H_{16}N_4O$ (%): C, 73.15; H, 4.91; N, 17.06. Found (%): C, 73.04; H, 4.93; N, 17.40. IR (KBr, cm^{-1}): 3400, 3070, 1587, 1566, 1501, 1460, 1235, 756, 695. ^1H NMR δ: 5.13 (s, 2H), 6.92–7.25 (m, 5H), 7.30–7.44 (m, 5H), 7.44–8.32 (m, 4H).

2.3. *Preparation of cis-$[Cu_2L_2Cl_4]\cdot 2CH_3CN$ (1)*

A solution of $CuCl_2\cdot 2H_2O$ (0.682 g, 4 mM) and anhydrous ethanol (15 mL) was added dropwise to a stirring solution of **L** (0.656 g, 2 mM) in boiling anhydrous ethanol (20 mL). The mixture was filtered into an acetonitrile solution (20 mL). The green crystalline solid that formed was isolated, washed with H_2O, and dried in vacuo to yield 0.603 g (75.2%) of the complex. Green single crystals suitable for X-ray analysis were obtained from an acetonitrile solution. Anal. Calcd for $C_{44}H_{38}Cl_4Cu_2N_{10}O_2$ (%): C, 52.44; H, 3.80;

N, 13.90. Found (%): C, 52.23; H, 3.49; N, 13.58. IR (KBr, cm^{-1}): 3410, 3072, 1603, 1506, 1463, 1236, 768, 702.

2.4. *Preparation of trans-[CoL_2Cl_2]·2H_2O·2CH_3CN (2)*

Complex **2** was prepared in 80.6% yield by a procedure similar to **1,** but using $CoCl_2·2H_2O$ instead of $CuCl_2·2H_2O$. The orange-yellow single crystals suitable for X-ray diffraction were obtained by evaporation from an acetonitrile solution. Anal. Calcd for $C_{44}H_{42}Cl_2CoN_{10}O_4$ (%): C, 58.41; H, 4.68; N, 15.48. Found (%): C, 58.77; H, 4.50; N, 13.91. IR (KBr, cm^{-1}): 3445, 3072, 1600, 1578, 1509, 1461, 1237, 766, 699.

2.5. *X-ray crystallographic study*

Well-shaped single crystals of **L**, **1** and **2** were selected for X-ray diffraction study. The unit cell parameters and intensity data were collected at 296(2) K on a Bruker SMART CCD diffractometer with a detector distance of 5 cm and frame exposure time of 10 s using graphite monochromated MoK_α ($\lambda = 0.71073$ Å) radiation. The structures were all solved by direct methods and refined on F^2 by full-matrix least squares using SHELXTL [20]. All non-hydrogen atoms were anisotropically refined. C10 of **L** and C21, C22 of **2** were disordered over two positions. The occupation factors of C10, C21 and C22 are 0.5. Due to disorder, the thermal parameters of partially occupied atoms and C–H distances in benzene ring are restrained during the refinement. All hydrogens of organic ligand were generated geometrically and allowed to ride on their respective parent, but were not

Table 1. Crystal data and structure refinement for **L**, **1** and **2**.

Compound	**L**	**1**	**2**
Empirical formula	$C_{20}H_{16}N_4O$	$C_{44}H_{38}Cl_4Cu_2N_{10}O_2$	$C_{44}H_{42}Cl_2CoN_{10}O_4$
Formula weight	328.37	1007.72	904.71
Crystal system	Monoclinic	Triclinic	Monoclinic
Space group	*P 21/c*	*P−1*	*C 2/c*
a (Å)	16.772(3)	10.7973(14)	27.326(3)
b (Å)	12.515(2)	11.1897(15)	8.2238(8)
c (Å)	8.2044(14)	11.5004(15)	23.409(2)
α (°)	90	92.467(2)	90
β (°)	95.801(2)	111.826(1)	124.411(1)
γ (°)	90	116.058(1)	90
V/Å^3	1713.3(5)	1122.7(3)	4340.0(7)
Z	4	1	4
D_c /Mg m^{-3}	1.273	1.490	1.385
T/K	296(2)	296(2)	296(2)
μ/mm^{-1}	0.082	1.235	0.574
Cryst. dimensions	0.15 × 0.12 × 0.10	0.17 × 0.15 × 0.11	0.17 × 0.14 × 0.12
No. of reflns. collected	12,524	8460	15,473
No. of unique reflns	3402	4301	4200
No. of parameters	227	282	284
Goodness-of-fit on F^2	1.059	1.047	1.064
R_1, wR_2 ($I > 2\sigma(I)$)	0.0607, 0.1726	0.0335, 0.0881	0.0452, 0.1305
R_1, wR_2 (all data)	0.0772, 0.1925	0.0417, 0.0926	0.0562, 0.1392
CCDC No	926304	923375	923376

Table 2. Selected bond distances (Å) and angles (°) for **L**, **1** and **2**.

L		**1**		**2**	
N4–C3	1.338(3)	Cu1–N1	2.202(2)	Co1–N2	2.110(1)
N4–C7	1.327(3)	Cu1–N2	2.004(2)	Co1–N4	2.139(2)
N1–N2	1.382(3)	Cu1–N4	2.014(2)	Co1–Cl1	2.466(7)
O1–C8	1.415(3)	Cu1–Cl1	2.293(4)	N1–N2	1.364(3)
O1–C9	1.379(3)	Cu1–Cl2	2.296(6)	O1–C14	1.412(3)
C7–N4–C3	117.10(20)	N1–N2	1.377(3)	O1–C15	1.381(3)
C1–N1–N2	107.34(17)	O1–C14	1.423(3)	N2–Co1–N4	76.25(7)
C2–N2–N1	107.56(17)	O1–C15	1.385(3)	N2A–Co1–N4	103.75(7)
C1–N3–C2	105.08(17)	N2–Cu1–N1	94.62(7)	N2–Co1–Cl1	90.01(6)
C9–O1–C8	117.17(18)	N4–Cu1–N1	77.63(7)	N2–Co1–Cl1A	89.99(6)
O1–C8–C1	107.69(18)	N2–Cu1–N4	172.23(8)	N4–Co1–Cl1A	91.23(6)
		N2–Cu1–Cl1	91.98(6)	N4–Co1–Cl1	88.77(6)
		N4–Cu1–Cl1	91.38(6)	N2–Co1–N2A	180.00(1)
		N1–Cu1–Cl1	119.29(6)	N4–Co1–N4A	180.00(1)
		N2–Cu1–Cl2	94.22(6)	Cl1–Co1–Cl1A	180.00(1)
		N4–Cu1–Cl2	89.36(7)		
		N1–Cu1–Cl2	112.75(6)		
		Cl1–Cu1–Cl2	126.81(3)		

Symmetry code: (A) $3/2-x$, $1/2-y$, $2-z$.

refined. Crystallographic data are summarized in table 1. Selected bond lengths and angles for **L**, **1** and **2** are listed in table 2. Molecular graphics were prepared using DIAMOND [21] and mercury programs [22]. Cambridge Crystallographic Data Center (CCDC) reference numbers 926304, 923375 and 923376 contain the supplementary crystallographic data in CIF format for the crystals reported in this article. These data can be obtained free of charge from The CCDC via www.ccdc.cam.ac.uk/data_request/cif.

2.6. *Hirshfeld surface calculations*

Hirshfeld surface analysis is gaining prominence as a technique in understanding the nature of intermolecular interactions within a crystal structure using a fingerprint plot. This allows easy identification of characteristic interactions throughout the structures or as a surface around the molecule [23]. The size and shape of a Hirshfeld surface reflect the interplay between different atoms and intermolecular contacts in a crystal. The distance from the Hirshfeld surface to the nearest atoms outside and inside the surface is characterized by the quantities d_e and d_i, respectively, and the normalized contact distance based on these, $d_{norm} = (d_i - r_i^{vdw})/r_i^{vdw} + (d_e - r_e^{vdw})/r_e^{vdw}$, is symmetric in d_e and d_i, with r_i^{vdw} and r_e^{vdw} being the van der Waals radii of the atoms [10]. The value of d_{norm} is negative or positive when intermolecular contacts are shorter or longer than r^{vdw}, respectively. The 2-D fingerprint plots, which are derived from the Hirshfeld surface, are complementary to these surfaces. They quantitatively summarize the nature and type of intermolecular contacts experienced by the molecules in the crystal. The 2-D fingerprint plots can also be broken down to give the relative contribution to the Hirshfeld surface area from each type of interaction, quoted as the "contact contribution". For a given crystal structure, the Hirshfeld surfaces as well as fingerprint plots are unique, and the number of unique Hirshfeld surfaces depends on the number of crystallographically independent molecules in the corresponding asymmetric unit [24].

3. Results and discussion

3.1. *Syntheses*

The asymmetrical 3-phenoxymethyl-4-phenyl-5-(2-pyridyl)-1,2,4-triazole (**L**) reacts with M^{2+} (M=Cu and Co) and Cl^- in molar ratios of 1 : 1 : 2 and 2 : 1 : 2 to form two neutral monomeric complexes, *cis*-$[Cu_2L_2Cl_4]\cdot 2CH_3CN$ (**1**) and *trans*-$[CoL_2Cl_2]\cdot 2H_2O\cdot 2CH_3CN$ (**2**). They are both stable in air. Yields for **1** and **2** are 75.2 and 80.6%, respectively.

3.2. *Crystal structure of L*

A perspective view of **L** with atom-numbering is shown in figure 1. Both bond lengths and angles in **L**, **1** and **2** are listed in table 2. In the structure of **L**, the central 1,2,4-triazole is surrounded by one pyridine, one phenyl, and one phenoxymethyl ring. The central 1,2,4-triazole is oriented at dihedral angles of 28.06(11)° and 83.57(9)° with respect to the pyridine and phenyl, respectively. The phenoxymethyl is highly disordered and the occupancy factor for C10 is fixed as 0.50. There is one C–H···N (C16–H16···N2 = 158° and H16···N2 = 2.60 Å) hydrogen bond and three C–H···π interactions in **L** (figures 1 and 2; table 3). These C–H···π interactions and intermolecular hydrogen bonds determine the dihedral angle of pyridine and triazole.

3.3. *Crystal structure of 1*

A projection of the structure of **1** was presented in figure 3, together with the atomic labeling system. Complex **1** crystallizes in the triclinic space group $P\bar{1}$ and there are two Cu(II) centers. Each Cu(II) is a distorted $[CuN_3Cl_2]$ trigonal bipyramid coordinated by two

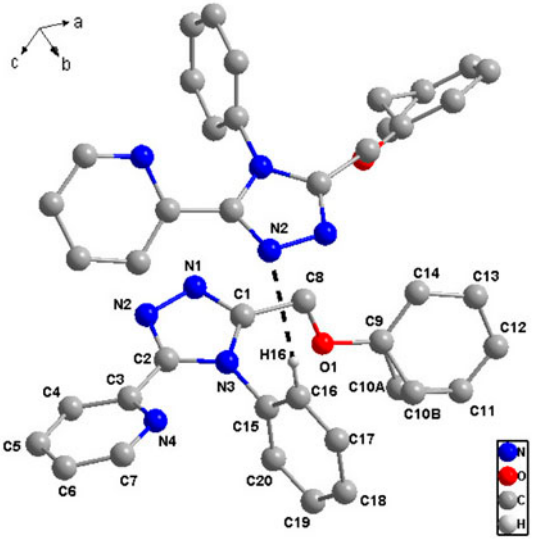

Figure 1. Projection of the structure of **L** with the atomic labeling system. Some hydrogens have been omitted for clarity.

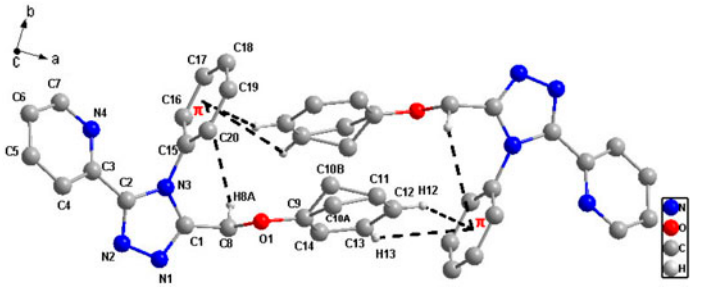

Figure 2. View of three edge-to-face C–H···π stacking interactions in **L**. Some hydrogens have been omitted for clarity.

Table 3. The hydrogen bonding geometry and π-stacking interaction for **L**.

D–H···A	D–H	H···A	D···A	<DHA
C16–H16···N2[a]	0.93	2.60	3.480(3)	158
C8–H8A···π	0.97	3.65	3.981(6)	103
C12–H12···π	0.93	3.69	4.286(4)	124
C13–H13···π	0.93	3.45	4.174(5)	137

Symmetry code: [a]x, $1/2-y$, $-1/2+z$.

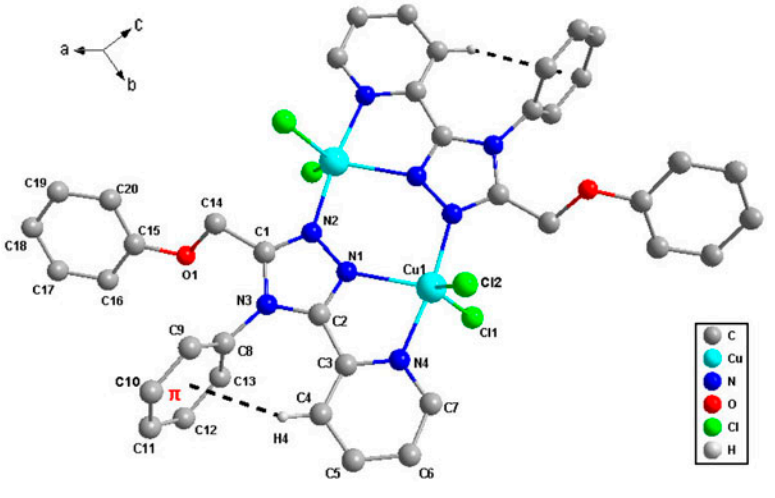

Figure 3. Projection of the structure of **1** with the atomic labeling system. Some hydrogens and acetonitriles are omitted for clarity.

Cl^- (Cl1, Cl2) and one nitrogen (N1) from **L** in the equatorial plane and N2 and N4 from two **L** in axial positions. Each **L** coordinates with two Cu(II) through N4 of pyridine and N1 and N2 of triazole, similar to the coordination in a related Cu(II) complex [17]. The Cu–N bond distances in the axial direction are shorter than that in the equatorial plane (table 2). The same feature has been observed in the similar complex [17]. The N2–Cu1–N4 linkages are almost linear (N2–Cu1–N4 = 172.23(8)°), whereas N1–Cu1–Cl1

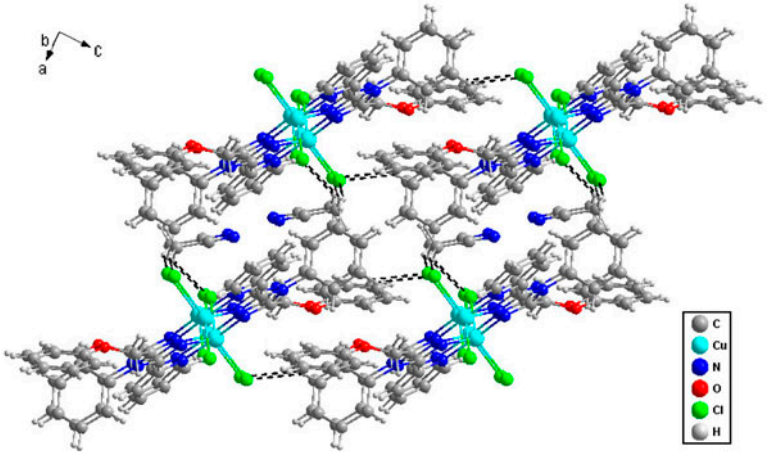

Figure 4. The crystal packing of **1** viewed along the b-axis showing hydrogen bonding.

Table 4. The hydrogen bonding geometry and π-stacking interaction for **1**.

D–H···A	D–H	H···A	D···A	DHA
C12–H12···Cl2[a]	0.93	2.80	3.619(3)	147
C22–H22C···Cl2[b]	0.96	2.76	3.644(5)	154
C4–H4···π	0.93	2.61	3.469(8)	153

Symmetry codes: [a]x, y, $1+z$; [b]$1-x$, $1-y$, $1-z$.

and N1–Cu1–Cl2 are bent, 119.29(6)° and 112.75(6)°, respectively. **L** in **1** is nonplanar. The triazole ring makes dihedral angles of 7.18(15)° and 77.90(19)° with the pyridine ring and phenyl ring, respectively. The crystal structure is further stabilized by weak edge-to-face C–H···π interactions involving C4–H4 and phenyl ring (C4–H4···π = 153° and H4···π = 2.61 Å). Moreover, there are two intermolecular C–H···Cl hydrogen bonds in **1** (figure 4 and table 4).

3.4. *Crystal structure of 2*

Figure 5 presents the structure of **2** with its atom numbering system. The crystal structure consists of one $[CoL_2]^{2+}$, two Cl^-, two lattice waters, and two acetonitriles. Unlike **1**, Co(II) in **2** is coordinated by four nitrogens from two **L** in the equatorial plane and two Cl^- in axial positions to form a distorted octahedral geometry. Each **L** coordinates to Co(II) through N4 of the pyridine and N2 of the triazole, similar to the coordination in a related complex [25]. The Co–N and Co–O distances are within the range observed for octahedral complexes [26]. However, the Co–N bond to the triazole nitrogen is 0.029 Å shorter than that to the pyridine nitrogen (table 2). This can be compared with those observed for ABPT complexes [27–29]. Similar to **1**, **L** in **2** is also nonplanar. The triazole ring makes dihedral angles of 6.84(18)° and 71.60(8)° with the pyridine and phenyl ring, respectively. C21 and C22 of acetonitrile are highly disordered (0.5, 0.5) and C22 is connected to the water molecule by C22B–H22E···O1 W hydrogen bonding.

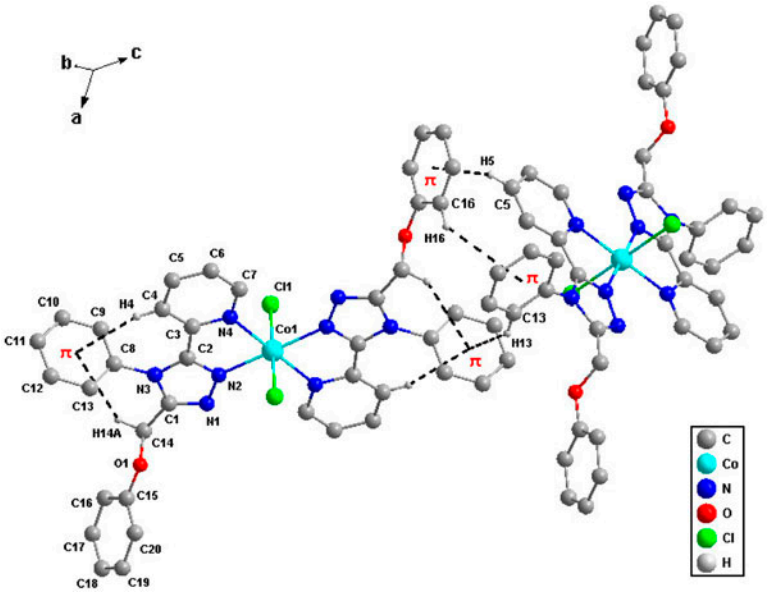

Figure 5. Projection of the structure of **2** with the atomic labeling system and edge-to-face C–H···π stacking interactions. Some hydrogens, acetonitriles and lattice waters are omitted for clarity.

Table 5. The hydrogen bonding geometry and π-stacking interaction for **2**.

D–H···A	D–H	H···A	D···A	<DHA
O1 W–H1 WA···Cl1[a]	0.87	2.55	3.310(5)	148
O1 W–H1WB···Cl1[b]	0.86	2.43	3.252(6)	159
C7–H7···N1[a]	0.93	2.61	3.429(3)	147
C9–H9···O1W	0.93	2.45	3.256(6)	145
C12–H12···Cl1[c]	0.93	2.83	3.686(4)	154
C22B–H22E···O1W[d]	0.96	2.26	3.217(4)	172
C4–H4···π	0.93	2.97	3.800(2)	149
C5–H5···π	0.93	2.69	3.545(3)	154
C13–H13···π	0.93	2.89	3.668(7)	141
C14–H14A···π	0.97	3.47	4.063(4)	122
C16–H16···π	0.93	3.26	4.008(6)	139

Symmetry codes: [a]$1/2-x, 3/2-y, -z$; [b]$x, -1+y, z$; [c]$1/2-x, -1/2+y, 1/2-z$; [d]$1/2-x, 1/2+y, 1/2-z$.

There are five kinds of intermolecular hydrogen bond interactions in **2** (table 5), which is associated with closer crystal packing. These hydrogen bond interactions include: (1) between water and Cl^- [O1 W–H1 WA···Cl1, O1 W–H1 WB···Cl1]; (2) between water and phenyl ring [C9–H9···O1W]; (3) between water and acetonitrile [C22B–H22E···O1W]; (4) between pyridine ring and triazole ring [C7–H7···N1]; (5) between phenyl ring and Cl^- [C12–H12···Cl1]. Different from **1**, **2** is further stabilized by five kinds of weak C–H···π interactions involving (1) C4–H4 and phenyl ring; (2) C5–H5 and phenoxymethyl ring; (3) C13–H13 and phenyl ring; (4) C14–H14A and phenyl ring; (5) C16–H16 and phenyl ring (figure 5). These hydrogen bonds and C–H···π interactions assemble the cation, anions, lattice water, and acetonitrile into a 3-D structure (figure 6).

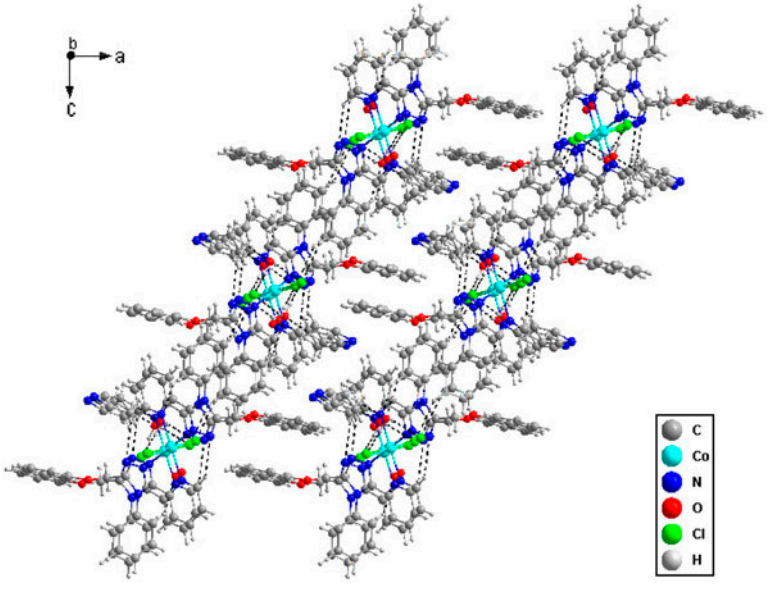

Figure 6. The crystal packing of **2** viewed along the b-axis showing hydrogen bonding.

3.5. *IR spectrum*

The IR spectrum of free **L** shows two medium bands at 1587 and 1566 cm^{-1}, attributable to pyridine ring vibrations. Upon pyridine coordination, the higher band is shifted by 15 wavenumbers. So, a band at 1603 cm^{-1} in the spectrum of **1**, and 1600, 1578 cm^{-1} in the spectrum of **2** can be assigned to the coordinated pyridine [27]. In **1** (or **2**), **L** uses one pyridine nitrogen and two triazole nitrogens (or one triazole nitrogen) for doubly-bidentate binding (or chelate binding), respectively, as confirmed by the structure determination. The medium and broadband centered at 3445 cm^{-1} for **2** is mainly attributed to H–O–H stretch of water, suggesting hydrogen bonding interactions [30]. The absence of similar high-frequency absorption for **1** suggests that there is no water within the structure. These features are in agreement with the results of the X-ray analyses.

3.6. *Thermal study*

The thermal behaviors of **1** and **2** were studied on a NETZSCH STA 449F3 thermal analyzer. Figures S1 and S2 show the TG profiles from 40 to 800 °C.

Two main thermal decomposition processes can be observed for **1**, the first weight loss of 8.84% at 100–180 °C corresponding to removal of two acetonitriles (calculated value is 8.14%). The second sharp weight loss above 230 °C is due to the decomposition of ligands with a mass loss of 68.66% (calculated value is 65.17%) to give the $CuCl_2$ residue.

The thermal profile of **2** is almost identical with that of **1**. The thermal decomposition profile of **2** indicates that it is stable upto 80 °C followed by a rapid weight loss from 80 to 137 °C corresponding to the loss of two lattice waters (Calcd 3.98%, obsd. 3.65%). The weight loss between 137 and 310 °C is attributed to the decomposition of two acetonitriles (Calcd 9.06%, obsd. 9.39%). Finally, a sharp weight loss occurs above 310 °C due to the

decomposition of the ligand (Calcd 72.60%, obsd. 70.58%) to give the $CoCl_2$ residue. The thermal decompositions of **1** and **2** are in agreement with their crystal structures.

3.7. *Molecular Hirshfeld surfaces*

Hirshfeld surface is a useful tool for describing the surface characteristics of the molecules. The molecular Hirshfeld surface (d_{norm}, shape index and curvedness) of 3-phenoxymethyl-4-phenyl-5-(2-pyridyl)-1,2,4-triazole in the present two complexes is shown in figure 7.

The d_{norm} surface is used for identification of very close intermolecular interactions. The value of d_{norm} is negative or positive when intermolecular contacts are shorter or longer than r^{vdW} (van der Waals (vdW) radii), respectively. The d_{norm} values are mapped onto the Hirshfeld surface by using a red–blue–white color scheme: where red regions correspond to closer contacts and negative d_{norm} value; the blue regions correspond to longer contacts and positive d_{norm} value; and the white regions corresponding to the distance of contacts is exactly the vdW separation and with a d_{norm} value of zero [10]. The red points on the d_{norm} surface of the three compounds correspond to significant hydrogen bonding interactions.

The shape index is most sensitive to very subtle changes in surface shape, the red triangles on them (above the plane of the molecule) represent concave regions indicating atoms π … stacked molecule above them, and the blue triangles represent convex regions

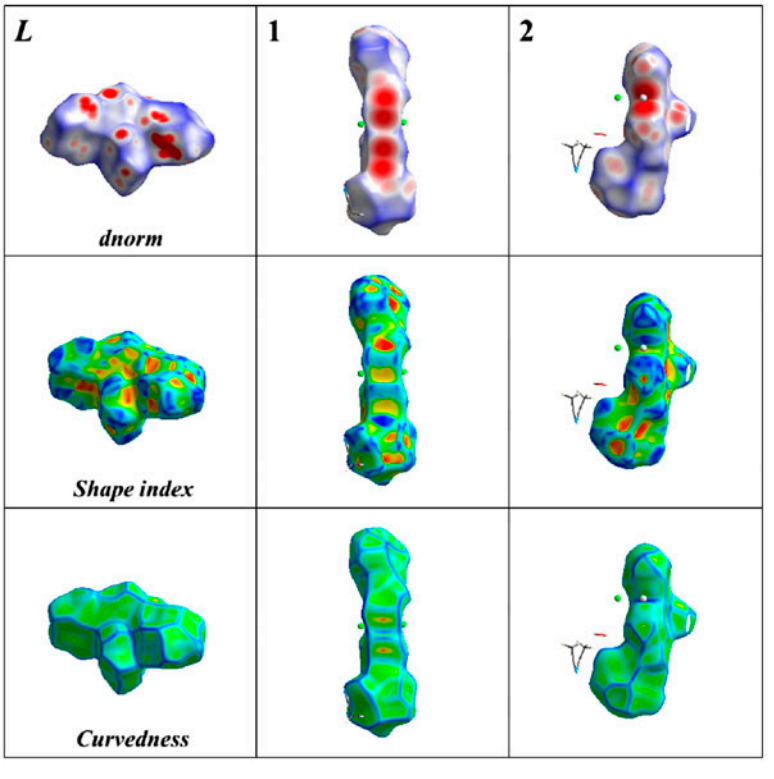

Figure 7. Molecular Hirshfeld d_{norm} surfaces, *shape index* and *curvedness* of 3-phenoxymethyl4-phenyl-5-(2-pyridyl)-1,2,4-triazole in **L**, **1** and **2**.

Table 6. Summary of the various contact contributions to the 3-phenoxymethyl-4-phenyl-5-(2-pyridyl)-1,2,4-triazole Hirshfeld surface area in **L**, **1** and **2**.

	L	**1**	**2**
H–H	54.4	39.2	41.5
C–H	20.6	22.6	32.3
N–H	16.3	7.3	13.7
O–H	3.4	3.2	4.5
H–M	–	0.3	0.1
N–M	–	–	2.8
Cl–M	–	2.8	–
N–N	0.2	4.7	–
N–C	1.7	4.5	0.3
N–O	–	0.2	0.3
C–C	3.5	2.5	0.1
C–O	–	1.7	0.5
H–Cl	–	9.2	2.9
N–Cl	–	1.6	0.8
C–Cl	–	0.4	–

indicating the ring atoms of these molecules inside these surfaces. In the case of the present three compounds, the red triangles are C–H$\cdots\pi$ intermolecular interactions, indicated by the "wings" in the upper left and lower right of the 2-D fingerprint plot (figure S3). They clearly show that complexation of **L** leads to increasing percentages of C–H$\cdots\pi$ interactions to the total Hirshfeld surfaces, actually, the percentages are 20.6, 22.6, and 32.3% for **L**, **1** and **2**, respectively (table 6). The information conveyed by the shape index are consistent with the 2-D fingerprint plots.

The curvedness is the measurement of "how much shape", the flat areas of the surface correspond to low values of curvedness, while sharp curvature areas correspond to high values of curvedness and usually tend to divide the surface into patches, indicating interactions between neighboring molecules. The large flat region delineated by a blue outline refers to the $\pi\cdots\pi$ stacking interactions. The curvedness of the present three compounds indicate no $\pi\cdots\pi$ stacking interactions.

The 2-D fingerprint plots complement the Hirshfeld surfaces, quantitatively summarizing the nature and type of intermolecular contacts experienced by molecules in the crystal. They are colored with a range from blue (relatively few points) through green (moderate points) to red (many points). Shown in figure 8 are the fingerprint plots of **L** in the present three crystals. It clearly shows the different intermolecular contacts experienced by **L**. The main intermolecular contact is H–H contact (shown in the middle of the scattered

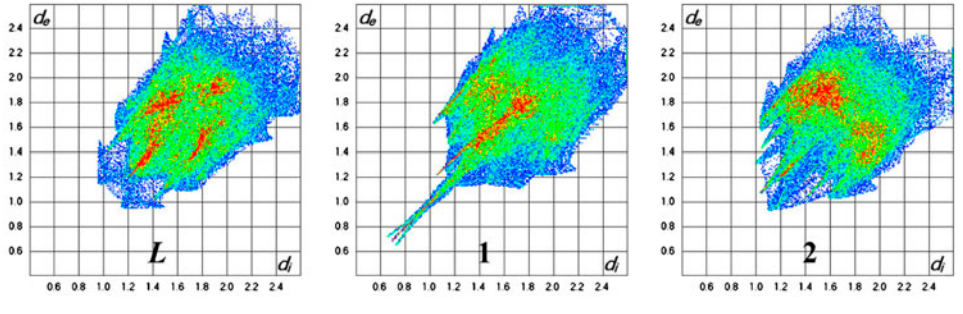

Figure 8. 2-D fingerprint plots of 3-phenoxymethyl-4-phenyl-5-(2-pyridyl)-1,2,4-triazole in **L**, **1** and **2**.

point in the 2-D fingerprint plots), but the complexation with metal ions leads to reduction of the H–H percentage to the total Hirshfeld surfaces. For **L**, **1** and **2** the percentage of H–H contacts is 54.4, 39.2, and 41.5%, respectively.

N–H interaction is one of the most significant contacts for these compounds. For **L**, N–H interaction is indicated by two large spikes (figure S3) and for the two complexes the percentage of N–H interactions decreased dramatically, from 16.3% in **L** to 7.3 and 13.7% in **1** and **2**, respectively. For the present three compounds, the percentage of O–H interactions are all less than N–H interactions, while for **1** the lower percentage of O–H and N–H contacts in contrast to **2** can be attributed to the high percentage of H–Cl contacts (9.2%).

All contacts are summarized in table 6.

4. Conclusion

Two new Cu(II) and Co(II) complexes with 3-phenoxymethyl-4-phenyl-5-(2-pyridyl)1,2,4-triazole (**L**), *cis*-$[Cu_2\mathbf{L}_2Cl_4]\cdot 2CH_3CN$ (**1**) and *trans*-$[Co\mathbf{L}_2Cl_2]\cdot 2H_2O\cdot 2CH_3CN$ (**2**) have been synthesized and characterized by IR, single-crystal X-ray diffraction, TGA, and Hirshfeld surfaces. **1** has a distorted trigonal bipyramidal $[CuN_3Cl_2]$ core with *cis* Cl^-, while **2** shows a distorted octahedron $[CoN_4Cl_2]$ with *trans* Cl^-.

The molecular Hirshfeld surface and fingerprint plots of **L**, **1** and **2** revealed that the complexation with transition metal ions results in the reduction of H–H and N–H contacts in receptor, and leads to strengthening of C–H contacts.

Supplementary material

Crystallographic data for the structures reported in this article have been deposited with the CCDC as supplementary publication Nos. CCDC 926304 (**L**), 923375 (**1**) and 923376 (**2**). Copies of the data can be obtained free of charge via www.ccdc.cam.ac.uk (or from the Cambridge Crystallographic Center, 12 Union Road, Cambridge CB2 1EZ, UK; Fax: t44 1223 336033; Email: deposit@ccdc.cam.ac.uk).

Acknowledgements

This work was funded by the National Nature Science Foundation of China (Nos. 20771059, 20771050 and 20971068) and the Natural Science Foundation of Jiangsu Province (BK2008371).

References

[1] M.H. Klingele, B. Moubaraki, K.S. Murray, S. Brooker. *Chem. Eur. J.*, **11**, 6962 (2005).
[2] M.H. Klingele, P.D.W. Boyd, B. Moubaraki, K.S. Murray, S. Brooker. *Eur. J. Inorg. Chem.*, 910 (2005).
[3] K.T. Potts. *Chem. Rev.*, **61**, 87 (1961).
[4] J.G. Haasnoot. *Coord. Chem. Rev.*, **200–202**, 131 (2000).
[5] M.H. Klingele, S. Brooker. *Coord. Chem. Rev.*, **241**, 119 (2003).

[6] U. Beckmann, S. Brooker. *Coord. Chem. Rev.*, **245**, 17 (2003).
[7] P.J. van Koningsbruggen. *Top. Curr. Chem.*, **233**, 123 (2004).
[8] D.R. Zhu, Y. Xu, Z. Yu, Z.J. Guo, H. Sang, T. Liu, X.Z. You. *Chem. Mater.*, **14**, 838 (2002).
[9] J.A. Kitchen, S. Brooker. *Coord. Chem. Rev.*, **252**, 2072 (2008).
[10] J.J. McKinnon, D. Jayatilaka, M.A. Spackman. *Chem. Commun.*, 3814 (2007).
[11] A.L. Rohl, M. Moret, W. Kaminsky, K. Claborn, J.J. McKinnon, B. Kahr. *Cryst. Growth Des.*, **8**, 12 (2008).
[12] Y.H. Luo, C.G. Zhang, B. Xu, B.W. Sun. *Cryst. Eng. Commun.*, **14**, 6860 (2012).
[13] Rigaku. *CrystalClear*, Tokyo (2005).
[14] J. Zhou, J. Yang, L. Qi, X. Shen, D. Zhu, Y. Xu, Y. Song. *Transition Met. Chem.*, **32**, 711 (2007).
[15] G.S. Matouzenko, A. Bousseksou, S.A. Borshch, M. Perrin, S. Zein, L. Salmon, G. Molnar, S. Lecocq. *Inorg. Chem.*, **43**, 227 (2004).
[16] S.P. Zhang, Z.D. Liu, S.C. Shao. *Acta Crystallogr.*, **E62**, o1279 (2006).
[17] Z.X. Wang, H.J. Xu, X.N. Gong, P.F Wu. *Chin. J. Inorg. Chem.*, **25**, 1492 (2009).
[18] W. Lu, D.J. Xie, Z.X. Wang, X. Shen, Y. Xu, D.R. Zhu. *Chin. J. Inorg. Chem.*, **26**, 717 (2010).
[19] K.J. Erwin. *Org. Chem.*, **23**, 1086 (1958).
[20] G.M. Sheldrick. *SHELXTL, Structure Determination Software Programs, (Version 5.10)*, Bruker Analytical X-ray Systems Inc., Wiskonsin, USA (1997).
[21] K. Brandenburg. *DIAMOND, Crystal and Molecular Structure Visualization, (Version 3.1b)*, Crystal Impact GbR, Bonn (2006).
[22] Cambridge Structural Database. *Mercury 2.3*, CCDC, Cambridge (2003–2004).
[23] J.J. McKinnon, A.S. Mitchell, M.A. Spackman. *Acta Crystallogr., Sect. B*, **60**, 627 (2004).
[24] J.J. McKinnon, F.P.A. Fabbiani, M.A. Spackman. *Cryst. Growth Des.*, **7**, 75 (2007).
[25] S.C. Shao, D.R. Zhu, X.H. Zhu, X.Z. You, S.S.S. Raj, H.K. Fun. *Acta Crystallogr., Sect. C*, 55, 1412(1999).
[26] P.B. Viossat, N.H. Dung, J.C. Lancelot, M. Robba. *Acta Crystallogr., Sect. C*, **40**, 935 (1984).
[27] U. Hartmann, H. Vahrenkamp. *Inorg. Chim. Acta*, **239**, 13 (1995).
[28] P.J. Kunkeler, P.J. van Koningsbruggen, J.P. Cornelissen, A.N. van der Horst, A.M. van der Kraan, A.L. Spek, J.G. Haasnoot, J. Reedijk. *J. Am. Chem. Soc.*, **118**, 2190 (1996).
[29] P.J. van Koningsbruggen, K. Goubitz, J.G. Haasnoot, J. Reedijk. *Inorg. Chim. Acta*, **268**, 37 (1998).
[30] K. Nakamoto. *Infrared Spectra of Inorganic and Coordination Compounds*, p. 166, Wiley, New York (1970).